Graft modification in bamboo cellulose nanofibrils: An effective option to improve compatibility and tunable surface energy

Carlos Alejandro Rodríguez-Ramírez
CIHIDECAR: Centro de investigaciones en Hidratos de Carbono
Alain Dufresne
PAGORA: Grenoble INP-Pagora
Norma Beatriz D'Accorso
Universidad de Buenos Aires Facultad de Ciencias Exactas y Naturales
Nancy Garcia (nancylis@gmail.com)
Centro de investigaciones en Hidratos de Carbono https://orcid.org/0000-0002-2587-5693

Research Article

Keywords: Cellulose nanofibrils, Chemically modified nanocellulose, Poly (lactic acid), Nanocomposite

Posted Date: March 1st, 2021

DOI: https://doi.org/10.21203/rs.3.rs-179487/v1

Graft modification in bamboo cellulose nanofibrils: An effective option to improve compatibility and tunable surface energy

C. A. Rodríguez-Ramírez[1,2], Alain Dufresne[3], Norma D´Accorso[1,2*], Nancy Lis Garcia[2*].

[1]Universidad de Buenos Aires, Facultad de Ciencias Exactas y Naturales, Departamento de Química Orgánica, Buenos Aires Argentina.

[2]CONICET-Universidad de Buenos Aires. Centro de Investigación en Hidratos de Carbono (CIHIDECAR). Buenos Aires, Argentina.

[3]Univ. Grenoble Alpes, CNRS, Grenoble INP, LGP2, F-38000, France.

*norma@qo.fcen.uba.ar

*nancylis@qo.fcen.uba.ar

Abstract

In this work, from an endemic and non-significant value-added bamboo argentine, nanofibrils (CNFs) of 20 nm in width were obtained. These nanofibrils were chemical modified in surface with three simple steps using a noncommercial low molecular weight polylactic acid. The success of modification was confirmed by FTIR, TGA, DSC and XRD analysis. The modified nanofibrils were taken up for changing surface properties in films based on commercial PLA. The results show that dispersive ($\boldsymbol{\gamma_S^D}$) component of films increase of 34.7 mN/m to 36.1 mN/m after the addition of modified nanofibrils from 2 to 5% in formulation of the films, comparing with a physical blend. Interesting others result in physical, mechanical, and thermal properties of the nanocomposites, were reported.

Keywords: Cellulose nanofibrils; Chemically modified nanocellulose; Poly (lactic acid); Nanocomposite.

1. Introduction

Renewable bio-based polymers and composites derived from natural resources are generating a great interest due to the depletion of fossil fuel resources and the negative environmental impact of fossil fuel-based plastic products (Kunaver et al. 2016; Maisa Milanez Ávila Dias Maciel, Kelly Cristina Coelho de Carvalho Benini, Herman Jacobus Cornelis Voorwald 2019; Souza et al. 2019). The use of biopolymers from renewable natural resources is therefore shifting to the mainstream owing to their sustainable nature, potential to decrease the reliance on fossil fuels, and availability (Bondeson and Oksman 2007; La Mantia and Morreale 2011).

Among the most promising biodegradable polymers stands out polylactic acid (PLA), because it has been known for several decades and has attracted much attention in both the academic and industrial sectors. The advantages of this polymer are due to the fact that it is an environmentally friendly plastic, commercially available, making it the most representative biodegradable and bio-based polymer (Scaffaro et al. 2017; Mao et al. 2019). PLA can be obtained through different methods of lactic acid monomers, i.e. direct polycondensation (DP), ring opening polymerization (ROP), solid state polymerization (SSP) and direct methods like azeotropic dehydration and enzymatic polymerization (Jamshidian et al. 2010). Besides its biobased character, it exhibits an excellent melt processability, a room temperature elastic modulus comparable to that of poly(ethylene terephthalate) and a tunable crystallinity (Carlmark et al. 2012). Cellulose is another biopolymer, which is among the most widely used and most abundant natural biopolymers that can be obtained from several naturals resources such as wood, some bacteria, fungi, and some algae (Corrêa et al. 2010). It is a linear macromolecular polysaccharide consisting of a long chain of glucose units linked by β-1, 4-glycosidic bonds (Wang et al. 2017). Its excellent properties such as biocompatibility, renewability, and non-toxicity combined with a low price and good mechanical properties make cellulose an attractive resource for a broad range of applications. Cellulose can be converted into nanocellulose (NC) through different approaches such as chemical, mechanical and biological treatments. NC can be extracted as cellulose nanocrystals (or whiskers) obtained by acid hydrolysis of a cellulose-rich substrate and cellulose nanofibrils (or CNFs) obtained by different combinations of

enzymatic, chemical and/or mechanical treatments of the starting raw material (Missoum et al. 2012). CNFs have been used as reinforcing material in a wide range of polymeric matrices, including PLA, thus preserving its bio-based nature. However, the hydrophilic nature of cellulosic plant fibers makes them difficult to disperse within the PLA matrix (Georgopoulos et al. 2005; Tingaut et al. 2010; Aitomäki et al. 2016; Ray and Sain 2016).

The hypothesis of this work is that the chemical modification of CNFs with low molecular weight PLA (PLA l) should improve the dispersion of modified CNFs in a hydrophobic polymer matrix such as PLA, promoting miscibility and interfacial adhesion between them. Therefore, the aim of this work was to prepare flexible biodegradable films from renewable natural resources and to develop composites with improved mechanical performance and thermal stability.

2. Experimental

2.1 Materials

L-Lactic acid (85-90%) was purchased from Biopack (Argentina). All the reagents: sodium hydroxide, hydrogen peroxide, p-toluenesulfonic acid monohydrate (TSA), benzoyl chloride, pyridine, thionyl chloride and solvents were obtained from commercial suppliers (Aldrich Co). Poly (lactic acid) pellets were provided by Shenzhen Bright China Industrial Co. Ltd. (Wuhan, China) (L-LA 90%, 10% D-LA). The number average molar weight (Mn = 77,000 g mol^{-1}) was determined by size exclusion chromatography (SEC). The weight average molar weight (Mw) and the polydispersity index were also determined and values of 200,000 g mol^{-1} and 2.6, respectively, were obtained. Prior to use, PLA was purified by dissolving it in dichloromethane and precipitating in methanol. All other materials were used without purification.

Preparation of cellulose nanofibrils (CNFs)

CNFs were produced following a procedure previously developed by Rodríguez Ramírez et al. (2019) (C. A. Rodríguez Ramírez et al. 2019). For the removal of waxy substances from the bamboo, 100 g of the sample was dewaxed in a Soxhlet apparatus with a 2:1 (v/v) mixture of ethanol:toluene for 6 h. Subsequently, lignocellulosic substances in

the samples were removed using a basic solution (NaOH 2%) at 75 °C for 1 h, and the process was repeated four times until the color of the sample became white. Thereafter, the residual material was filtered and rinsed with deionized water four times until neutral pH. Next, residual hemicelluloses and pectin were removed by treating the sample with hydrogen peroxide solution (10%) at 60 °C for 6 h. After these chemical treatments, a bamboo cellulose dispersion (2 wt%) was prepared by adjusting the concentration of the dispersion with distilled water and mixed with an IKA high-shear mixer (T-T18 ULTRA TURRAX Basic) at 15,000 rpm speed. pretreated bleached fibers were disintegrated in a microfludizer process in a MASUKO® (MKCA6-2, Masuko Sanguo, Japan) and were passed through the device up to 60 times. The gap between the disks was adjusted to 9 µm. The dispersion CNF were centrifuged at 10,000 rpm to reduce its water content and kept wet in the fridge.

Synthesis of poly(lactic acid) with low molecular weight (PLA1)

The synthesis of PLA1 was performed according to a previously described method (Fukushima et al. 2005; Minh et al. 2013). The synthesis was carried out by condensation of the L-lactic acid (LLA), using p-toluenesulfonic acid (TSA) as catalyst. In a three-neck round bottom flask, 100 mL LLA and 0.4 g TSA were mixed. Then, the mixture was heated to 175 °C at reduced pressure to start the polycondensation. After a period of 24 hours of polycondensation, the reaction was stopped; the products were dissolved in chloroform and precipitated in methanol. Finally, the precipitate was filtered and dried in a vacuum oven at 40 °C for 48 hours. The number average molar weight (Mn = 10,000 g mol-1) was determined by size exclusion chromatography (SEC). The weight average molar weight (Mw) and the polydispersity index were also determined and values of 14,000 g mol-1 and 1.4, respectively, were obtained. PLA1 was characterized by physical, spectroscopic, and thermal methods.

Chemical functionalization of CNFs.

A previously reported procedure (García et al. 2012) was used that consists in three reaction steps (**Scheme 1**). The first step is the protection of the hydroxyl groups of PLA1 through a benzoylation reaction (PLA1Bz), the second step involves the activation of

carboxyl groups with thionyl chloride (PLA1BzCl), and these latter groups react immediately with the cellulose nanofibrils (PLA1Bz-g-CNF) during the third step.

Synthesis of PLA1Bz

PLA1 (1.0 g) and chloroform (20 mL) were mixed in a three-neck flask. Then, 1 mL benzoyl chloride and 1 mL pyridine were added. After 24 h of agitation at 45 °C, the mixture was subjected to few extractions with solvents and precipitated with methanol. The mixture was filtered, and the solid (PLA1Bz) was dried in a vacuum at 40 °C for 24h.

Synthesis of PLA1BzCl

The activation of carboxyl groups was achieved by dissolving 1.0 g of PLA1Bz in 60 mL of a 1:1 mixture dichloromethane:toluene at 70 °C in a three-neck flask. Then thionyl chloride (0.2 mL) and 0.5 mL of triethylamine (TEA) were added and submitted to constant stirring during 3 h. The product obtained was named PLA1BzCl and it was used without further purification.

Surface chemical modification of cellulose nanofibrils

The chemical modification of CNFs was performed in a round-bottomed reaction flask under reflux (48 h) under constant mechanical stirring in toluene medium. To suspend CNFs in toluene, a solvent exchange procedure consisting in several successive centrifugation and redispersion operations was used (water to acetone, and then acetone to toluene, both four times). Then, to perform esterification of CNFs (0.19 g) previously sonicated in toluene (10 mL) during 10 min was added to PLA1BzCl. PLA1Bz-g-CNF was purified and stored for further analysis and the preparation of nanocomposites.

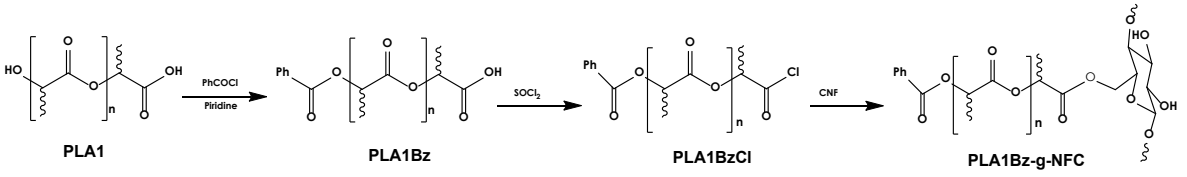

Scheme 1. Chemical modification performed on CNFs to obtain PLA1-g-CNF.

Preparation of PLA/PLA1Bz-g-CNF and PLA/PLA1Bz/CNF

After purification of products PLA1, PLA1Bz and PLA1Bz-g-CNF, nanocomposites were prepared by solution casting using chloroform as solvent. Initially, high molecular PLA (Table N° 1) was dissolved in chloroform (12 mL) using a magnetic stirrer, and then PLA1Bz-g-CNF was added. The filler content (PLA1Bz-g-CNF) in nanocomposites was varied from 0 to 5% based on the total weight of PLA. Subsequently, the nanocomposites were dried completely at 50 °C under vacuum for 48 hours. For comparison purpose a blend of PLA, PLA1Bz and CNFs (PLA/PLA1Bz/CNF) was prepared using similar procedure. Table 1 shows the composition of the different materials.

Table 1. Composition of the PLA/PLA1Bz-g-CNF and PLA/PLA1Bz/CNF nanocomposites.

	%PLA	% PLA1Bz-g-CNF	%PLA1Bz/CNF
1	100	-	-
2	98.0	2.0	-
3	97.0	3.0	-
4	96.0	5.0	-
5	98.0	-	2.0

2.3 Characterization

2.3.1. Scanning electron microscopy (SEM)

Nanofibrils were sonicated for 30 seconds and deposited on microscope glasses and vacuum dried at 40°C for 24 h. Samples were coated with gold using an ion sputter coater and observed by using a scanning electron microscope Zeiss Supra 40 with field emission gun operated at 3 kV.

2.3.2 Molecular weight determination

PLA molecular weight was determined by Size Exclusion Chromatography (SEC) on a Waters 600 at 31 °C, through a Styragel HR 4 THF- 7.8 x 300 mm - (5K-600K) column

and a refractive index detector 2414 at a flow rate of 1 mL min^{-1}, using polystyrene standards.

2.3.3 Fourier-transform infrared spectroscopy (ATR-FTIR)

Attenuated total reflection Fourier Transform Infrared (ATR-FTIR) spectroscopy (Nicolet IS50) was used to follow the impact of the different reactions and to compare grafted to unmodified CNFs and nanocomposites, recording changes in functional groups induced by the modification of nanocellulose. Spectra were collected in the range 4000 cm^{-1} – 500 cm^{-1}, at a resolution of 4 cm^{-1}.

2.3.4 X-ray diffraction analysis

A Siemens D 5000 X-ray diffractometer was used to observe the possible change in X-ray diffraction patterns during the reactions and to compare grafted to unmodified CNFs. X-ray generator voltage and current were 40 kV and 30 mA, respectively. The radiation was Cu Kα with wavelength 1.54 Å. The diffraction patterns were obtained at room temperature in the range of 2θ between 14 ° and 21 ° by step of 0.02 °.

2.3.5 Thermo-gravimetric analysis (TGA)

Thermogravimetric tests were performed using Shimadzu TGA-51H. Approximately 5 mg of each sample was subjected to heating from 30 °C to 500 °C at a rate of 10 °C/min and nitrogen flow 30 mL/min. The weight loss of the materials was calculated on dry basis and the different degradation phases were noted.

2.3.6 Differential scanning calorimetry (DSC)

Calorimetric measurements were made on a TA Q20 differential scanning calorimeter in a dry nitrogen atmosphere. Indium standard was used for calibration. Samples of 5−10 mg were placed in the DSC pan. Samples were first heated to 200 °C and held at that temperature for 10 min to remove the thermal history. Then, the samples were cooled to − 25 °C at a rate of 10 °C/min, held for 10 min, and heated again to 200 °C at 10 °C/min. The Tg value was taken as the midpoint of the transition. The degree of

crystallinity (X_c) for PLA, PLA/PLA1Bz-g-CNF and PLA/PLA1Bz/CNF nanocomposite films was calculated using Eq. (1).

$$X_c = \left[\frac{\Delta H_m - \Delta H_c}{\Delta H_m^c}\right] x \frac{100}{W_{PLA}} \quad (1)$$

Where ΔH_m and ΔH_c represent the melting enthalpy and cold crystallization enthalpy, respectively, ΔH_m^c is the melting enthalpy for 100% crystalline PLA which was set to 93.6 J/g (Quero et al. 2012). W_{PLA} depicts the weight fraction of PLA in the nanocomposite sample.

2.3.7 Contact angle measurements

Contact angle tests were carried out with a dynamic contact angle tensiometer at room temperature, using the sessile drop measurement technique. For each test 10 µL of various liquids: diiodomethane, formamide and water, were used. The sliding angle (α) which is defined as the minimum angle from horizontal required for a water droplet to roll was determined. Measurements of α were performed trigonometrically by determining the minimum altitude for a water droplet to start rolling. For a given sample, the contact angle was measured in ten different locations on the surface (for each location, the value of the contact angle at the left and right sides of the drop was recorded). The contact angle at equilibrium for pure liquids having different polarities was used to calculate the dispersive and polar contributions to the surface energy according to the approach proposed by Owens and Wendt (Owens et al. 1969; Adamson and Gast 1990) by using Eq. (2). The total, dispersive and polar components of these liquids are listed in **Table 2**.

Table 2. Surface tension contribution (total, $\boldsymbol{\gamma}$, dispersive, $\boldsymbol{\gamma^D}$, and polar, $\boldsymbol{\gamma^P}$, surface energy) for liquids used for contact angle measurements.

	Water	**Formamide**	**Diiodomethane**
$\boldsymbol{\gamma}$ **(mN m^{-1})**	72.8	58.0	50.8
$\boldsymbol{\gamma^D}$ **(mN m^{-1})**	21.8	39.0	49.5
$\boldsymbol{\gamma^P}$ **(mN m^{-1})**	51.0	19.0	1.3

$$\gamma(1+cos\theta) = 2\sqrt{\gamma_L^D \gamma_S^D} + 2\sqrt{\gamma_L^P}\gamma_S^P \qquad (2)$$

where γ, γ^D, and γ^P are the total, dispersive, and polar surface energy, respectively. Subscripts L and S refer to the liquid droplet and the solid surface, respectively, and θ denotes the contact angle between the solid surface substrate and the liquid droplet. According to Eq. (3):

$$\frac{\gamma_L(1+cos\theta)}{2.\sqrt{\gamma_L^D}} = \sqrt{\gamma_S^D} + \sqrt{\frac{\gamma_L^P}{\gamma_L^D}}\sqrt{\gamma_S^P} \qquad (3)$$

by plotting $[\gamma_L(1+cos\theta)]/[2(\gamma_L^D)^{0.5}]$ vs. $(\gamma_L^P/\gamma_L^D)^{0,5}$ a straight line should be obtained, where $(\gamma_S^P)^{0,5}$ and $(\gamma_s^D)^{0,5}$ are the slope and the y-axis intercept, respectively, for each of the materials tested. The total surface energy of the nanocomposite is easily obtained by using Eq. (4):

$$\gamma_S = \gamma_S^D + \gamma_S^P \qquad (4)$$

2.3.8 Mechanical characterization

Uniaxial tensile tests were performed on dumbbell shape samples cut out from the PLA matrix and the PLA, PLA/PLA1Bz, PLA/PLA1Bz-g-CNF and PLA/PLA1Bz/CNF composites films with an INSTRON dynamometer 5982. Stress–strain curves were obtained at 5 mm/min and using a load cell of 1 kN in accordance with the ASTM D638 standard. The specimen dimension was 8 x 0.3 x 30 (in mm) denoting, respectively, the width, thickness and length of the samples. Between 6 and 8 samples-were evaluated and conditioned at 23 ◦C and 60% RH for at least 48 h before testing. From these tests, the average Young's modulus, tensile strength, and strain at break and their deviations were calculated. The work of fracture was also estimated from the area under the stress-strain curve before rupture.

3. Results and discussion

3.1. Characterization of Cellulose Nanofiber

3.1.1. Morphology and structure of Cellulose Nanofibrils

In Figure 1A and 1A is shown the SEM micrographs nanofibrils morphology. The diameter of nanofibrillated cellulose from bamboo was determined by digital image analysis from FE-SEM micrographs with its own internal analytics software of Zeiss Supra 40, as presented in the Fig. 1. The average diameter of CNFs was about 20 ± 2nm (a minimum of 50 measurements was performed).

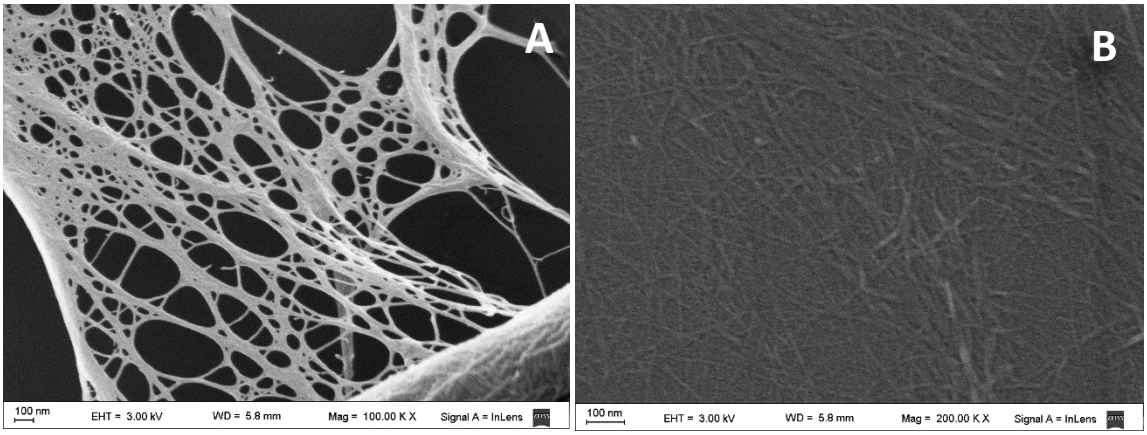

Fig. 1 FESEM of A, B. CNFs Tacuara Cane, with different magnifications, A: 100.00 KX and B: 200 KX

Both figures display a classical web-like network structure in which the fibrils occur as randomly entangled cellulosic nanofilaments. Figure 1B shows homogeneous dispersion and uniform dimensions the diameter range of cellulose nanofibrils obtained. Similar structure was observed by authors were reported. (Kwak et al. 2018; Rol et al. 2018).

3.2 Characterization of grafting of PLA1 on CNFs

3.2.1 Infrared Spectroscopy Measurements

Figure 2A shows the FTIR spectra for the different materials, while clear traces of modification can be noticed in panels B and C.

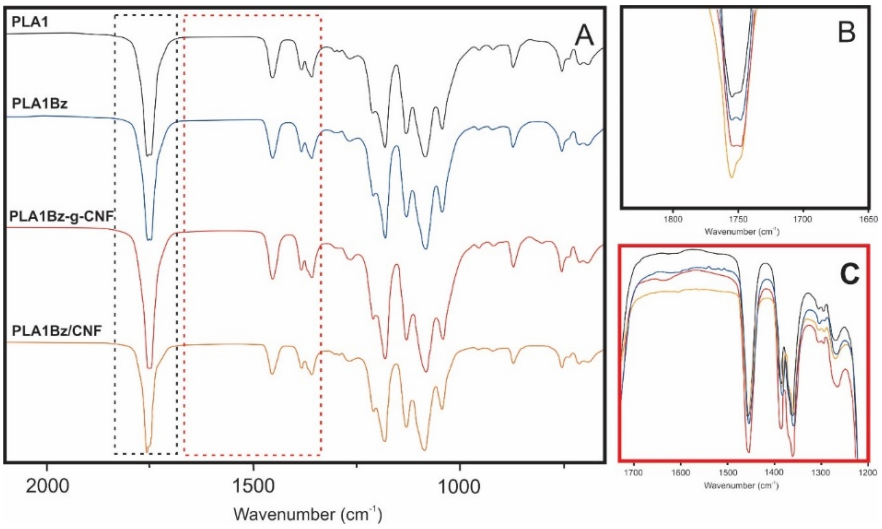

Fig. 2 (A) ATR-FTIR for PLA1, PLA1Bz, PLA1Bz-g-CNF and PLA1Bz/CNF; (B) expanded view of the band near 1750 cm^{-1}; (C) expanded view of the spectra in the 1700-1200 cm^{-1} wavenumber range.

All spectra show a clearly defined band at 1750 cm^{-1} (Figure 2A), which can be attributed to the stretching of carbonyl groups of the ester function. However, when zooming in on this wavenumber zone (Figure 2B), changes in intensity can be observed. By comparing PLA1Bz and PLA1Bz-g-CNF, these vibration peaks are attributed to new ester groups formed during chemical modification (Trinh and Mekonnen 2018; Gorade et al. 2019). On the other hand, the widening of the band observed at 1637 cm^{-1} (Figure 2C) is attributable to the presence of phenyl neighboring the carbonyl group (Sajan et al. 2006; Ly et al. 2008; Paquet et al. 2010).

3.2.2 Thermogravimetric analysis (TGA).

The TGA curves for PLA1, PLA1Bz, PLA1Bz-g-CNF and PLA1Bz/CNF are shown in Figure 3.

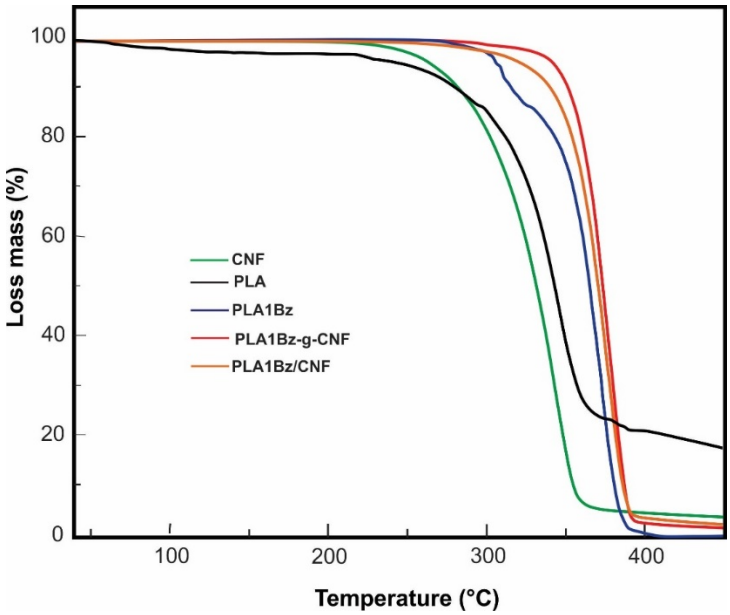

Fig. 3 Thermogravimetric analysis for PLA1, CNF, PLA1Bz, PLA1Bz-g-CNF, and PLA1Bz/CNF

From TGA analysis it is worth noting the highest thermal stability for PLA1Bz-g-CNF (red line in Fig. 3) in comparison with the precursor materials (PLA1 and PLA1Bz). PLA1Bz-g-CNF exhibits a 50 °C increase in the degradation temperature compared to neat CNFs. This phenomenon is attributable to the fact that the grafted product generates an effective wrapping due to the hydrogen bond interactions between PLA1 chains and CNFs, which acts as a protective layer inhibiting the degradation of the material (Wu et al. 2016) and demonstrates the success of the grafting.

In the thermogram to PLA1Bz (blue line) is observed two important losses. The first one, between 304 and 310 °C, was assigned to the degradation of the carboxyl group. It is reasonable not to observe this step on the thermogram for PLA1, because in this polymer is stabilized by the formation of hydrogen bonds between the carboxyl group with the end hydroxyl group of another PLA1 chain (Kopinke et al. 1996). The second degradation process could be due to several decomposition reactions. The thermal degradation of PLA1 is mainly associated with the hydrolysis of the ester groups and it is accelerated by the end groups (–COOH) (Piemonte and Gironi 2013).

The TGA curve for CNF (green line) shows two degradation steps, one below 100 °C and a maximum loss rate at 285 °C. The first step corresponds to depolymerization, dehydration and decomposition of glycosidic units starting at 100 ° C and reaching its maximum value (Tmax) at 285 °C. During this degradation process the residual hemicellulose and lignin contained in the material are broken down (Oun and Rhim 2016; C. A. Rodríguez Ramírez et al. 2019).

The original PLA1 degrades in a single stage within a narrow temperature range (307-377 °C) with a maximum degradation rate at 358 °C, in agreement with literature reports (Kopinke et al. 1996).

3.2.3 Differential scanning calorimetry (DSC)

Figure 4 shows the DSC thermograms for PLA1, protected PLA (PLA1Bz), grafted nanofibrils (PLA1Bz-g-CNF) and PLA1Bz/CNF blend. The main characteristics of the observed thermal events are reported in Table 3.

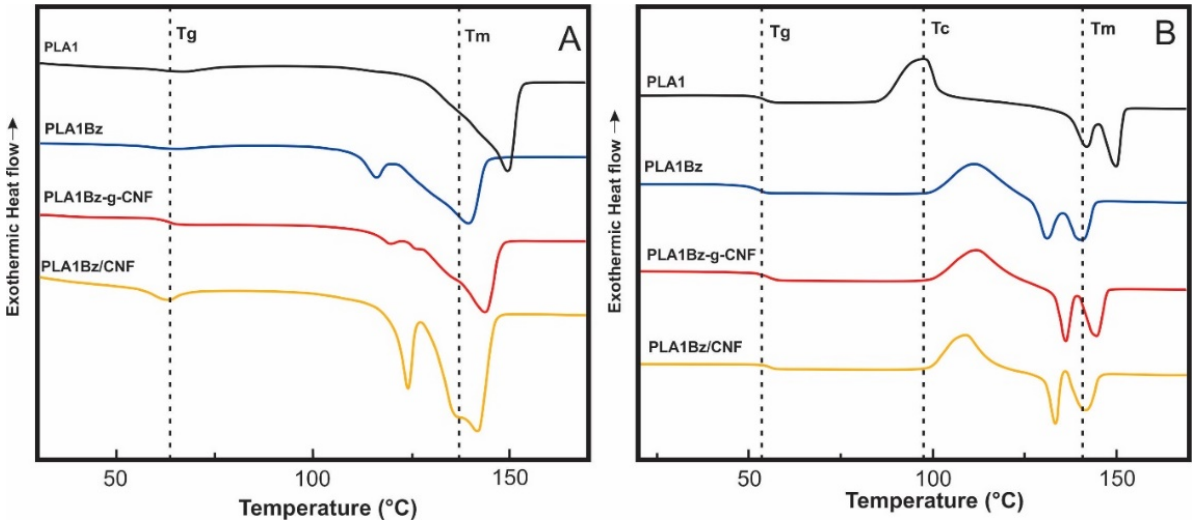

Fig. 4 DSC analysis for PLA1, CNF, PLA1Bz, PLA1Bz-g-CNF, and PLA1Bz/CNF: (A) first heating scan, and (B) second heating scan.

Table 3. Thermal transition temperatures (T_g = glass transition temperature; T_m = melting temperature; T_c = crystallization temperature), enthalpy of fusion (ΔH_m), enthalpy of crystallization (ΔH_c), and degree of crystallinity (X_c) for PLA1, PLA1Bz, PLA1Bz-g-CNF and PLA1Bz/CNF.

Sample	First Heating Scan				Second Heating Scan					
	T_g (°C)	T_m (°C)	ΔH_m (J/g)	X_c (%)	T_g (°C)	T_c (°C)	ΔH_c (J/g)	T_m (°C)	ΔH_m (J/g)	X_c (%)
PLA1	70.2	149.3	48.9	52.2	54.1	96.9	34.9	149.9	38.1	40.7
PLA1Bz	57.9	138.9	44.7	47.8	52.0	111.4	28.2	140.5	28.0	29.9
PLA1Bz-g-CNF	62.9	143.5	43.7	46.7	54.8	111.6	35.8	136.3	31.0	33.1
PLA1Bz/CNF	59.6	141.4	46.7	49.9	55.2	111.0	33.5	133.8	39.8	42.5

The melting point observed for PLA1 during the first heating scan was similar to that observed during the second heating scan, indicating that the size of the crystallites was comparable. However, a lower degree of crystallinity was noted for PLA1 during the second heating scan (Xc = 41%) compared to that reported during the first heating scan (Xc = 52%) suggesting that the heating rate used for DSC experiments was too fast to fully crystallize the polymer . In addition, part of the crystallites that were melting during the second heating scan were formed during this experiment as shown by the crystallization peak. This lower crystallinity of the polymer prior to the second heating scan is reflected through a lower glass transition temperature (54.1 °C vs. 70.2 °C for the second and first heating scan, respectively). The protection of the hydroxyl groups of PLA1 through benzoylation reaction (PLA1Bz) induced a decrease in both the melting temperature and the degree of crystallinity, and concomitant decrease in Tg value. This hindrance to crystallization induced by the benzoylation reaction was also reflected through a higher crystallization temperature.

Similar trends, i.e. lower degree of crystallinity and lower Tg values were observed for PLA-grafted on CNFs (PLA1Bz-g-CNF) and the physical mixture (PLA1Bz/CNF) when comparing the thermal characteristics between the first and second heating scan, but a lower melting point was also noted during the second heating scan. The presence of CNFs induced an increase in both the Tg value and degree of crystallinity of PLA as already reported (Suryanegara et al. 2009; Lv et al. 2017; Shojaeiarani et al. 2019). Moreover, PLA-grafted on CNFs

shows a higher Tg (62.9 °C during the first heating cycle), than that of the physical blend (59.6 °C) and that of PLA1Bz (57.9 °C). The same observation was reported for the melting temperature, which was 143.5 °C for the grafted product, 138.9 °C for PLA1Bz, and 141.4 °C for the blend. No significant variation in the crystallization temperature for PLA1Bz-g-CNF and PLA1Bz/CNF was observed, but when comparing the enthalpy of crystallization of the materials, an increase was reported when adding of CNFs.

3.2.4 X-ray diffraction (XRD) analysis

Figure 5 shows the XRD patterns for PLA1, PLA1Bz, PLA1Bz-g-CNF, and PLA1Bz/CNF. The magnitude of the diffraction peak located at 2θ = 16.6° for PLA1Bz/CNF is significantly higher than for PLA1Bz-g-CNF. This observation agrees with the higher degree of crystallinity reported from DSC experiments. When comparing the diffraction peaks located at 2θ = 16.6° and 2θ = 19.0° for PLA1Bz-g-CNF with respect to other materials, a slight shift towards higher 2θ values is observed, attributed to the effect of the grafting on the crystallization of PLA, confirming the success of the grafting reaction already reported from spectroscopic and thermal analysis (Yu et al. 2008; Inácio et al. 2020).

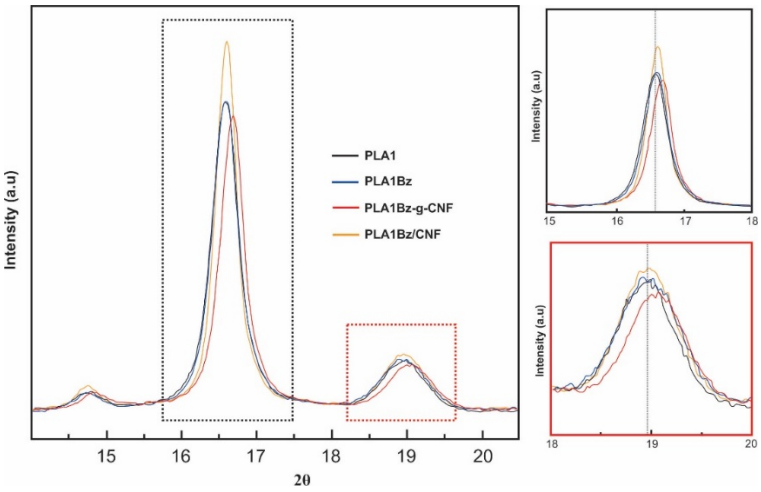

Fig. 5 XRD patterns for PLA1, PLA1Bz, PLA1Bz-g-CNF and PLA1Bz/CNF.

3.3. Characterizations of nanocomposites

3.3.1 Thermal properties and crystallinity of nanocomposites

TGA experiments showed the effect of adding PLA1Bz-g-CNF on the thermal properties of PLA films. For comparison, a PLA/PLA1Bz/CNF blend (composition 0.2% of nanofibrils) was tested and all results are illustrated in **Figure 6**.

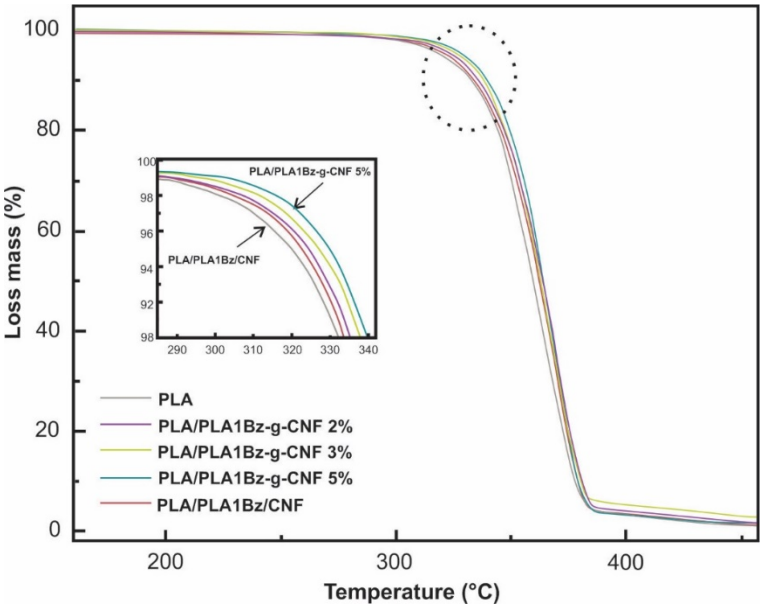

Fig. 6 TGA curves for neat PLA, PLA/PLA1Bz-g-CNF and PLA/PLA1Bz/CNF films.

All samples were thermally stable up to 285°C, while above this temperature, the bionanocomposites started to undergo decomposition. A slight increase in the onset decomposition temperature was observed when adding PLA1Bz-g-CNF to PLA. When the PLA1Bz-g-CNF content was 5% the onset decomposition temperature increased by almost 7 °C compared with neat PLA. It is well-known that enhanced thermal stability of the host polymer results from favorable filler/matrix interactions. This result shows the successful modification of the nanofibrils and improved filler/matrix compatibility. On the other hand, no significant increase in decomposition temperature was reported for the composite based on PLA1Bz/CNF blend compared to PLA1Bz-g-CNF 2% (360 °C vs. 363 °C), which is attributed to the poor compatibility and low level of dispersion of the blend in the polymer matrix (Aouat et al. 2018).

3.3.2 DSC experiments for PLA and PLA nanocomposites

The thermal characteristics and crystallization behavior of neat PLA film and nanocomposites were investigated by DSC. The corresponding thermograms are presented in **Figure 7**. In addition, the values of glass transition temperature (Tg), cold crystallization temperature (Tc), melting temperature (Tm), enthalpy of crystallization (ΔHc), enthalpy of melting (ΔHm) and degree of crystallinity (Xc) of the films are given in **Table 4.**

Tabla 4. Thermal transition temperatures (T_g = glass transition temperature; T_m = melting temperature; T_c = cold crystallization temperature), enthalpy of fusion (ΔH_m), enthalpy of crystallization (ΔH_c), and degree of crystallinity (X_c) for neat PLA and PLA nanocomposites.

Material	Tg (°C)	Tc (°C)	ΔHc (J/g)	Tm (°C)	ΔHm (J/g)	χ_c (%)
Neat PLA	61.4	109.2	29.9	169.8	33.2	3.6
PLA/PLA1Bz -g-CNF 2%	61.2	111.5	32.7	170.1	35.0	2.5
PLA/PLA1Bz -g-CNF 3%	61.2	111.6	32.4	165.3	34.6	2.3
PLA/PLA1Bz -g-CNF 5%	60.9	110.9	29.3	169.8	31.4	2.4
PLA1Bz /CNF/PLA (BLEND)	61.6	111.0	37.8	170.0	42.7	5.3

The glass transition temperature (Tg) for neat PLA was about 61.4 °C, and the cold crystallization peak was observed in **Figure 7** around 109.2 °C. No significant change in the Tg value was observed for the nanocomposites, regardless of the filler content, and the cold crystallization temperature (Tc) was marginally shifted by only 2 °C towards higher temperatures compared with neat PLA film.

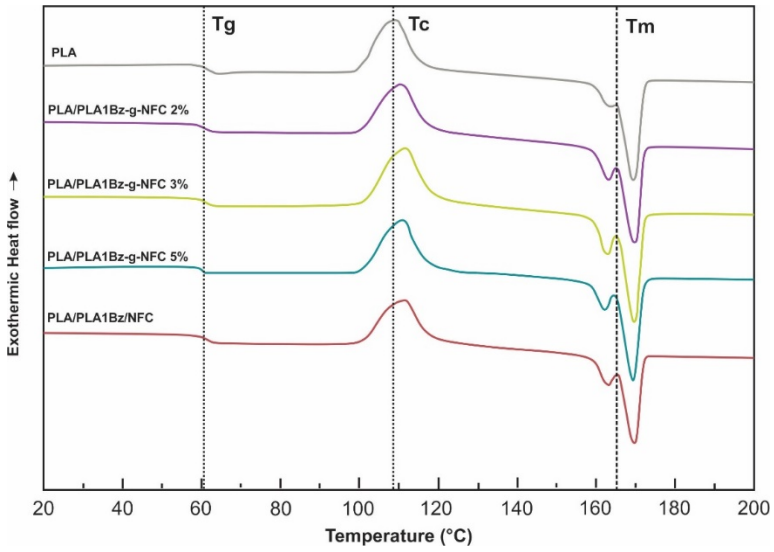

Fig. 7 DSC thermograms for neat PLA and PLA nanocomposites.

Meanwhile, when adding CNFs in PLA, an increase of the enthalpy of crystallization was observed, except for PLA/PLA1Bz-g-CNF 5%. This increase was particularly marked for the physical blend, which showed therefore an easier crystallization for PLA. The melting point remained globally constant for nanocomposites compared to neat PLA, except for PLA/PLA1Bz-g-CNF 3%. Regarding the degree of crystallinity (Xc), it decreased from 3.6% for the neat PLA to about 2.4% for nanocomposites reinforced with PLA1Bz-g-CNF, whereas it increased 5.3% when using PLA1Bz/CNF. It is worth noting that this crystallinity corresponds to the crystalline phase formed during the cooling cycle at 10°C/min and initially present before the second heating scan according to Eq. (1). CNFs are well-known for acting as a heterogeneous nucleating agent (Zamir et al. 2018; Shojaeiarani et al. 2019), which is effectively observed for the physical blend, but it seems that PLABz-grafted CNFs did not play this role.

3.3.3 Mechanical properties

The mechanical properties, such as Young's modulus, tensile strength, elongation at break and work of fracture were evaluated from the stress–strain curves. Typical stress–strain curves for pure PLA and nanocomposites with different PLA1Bz-g-CNF contents

and PLA1Bz /CNF blend are shown in **Figure 8** and the related data are summarized in **Table 5**.

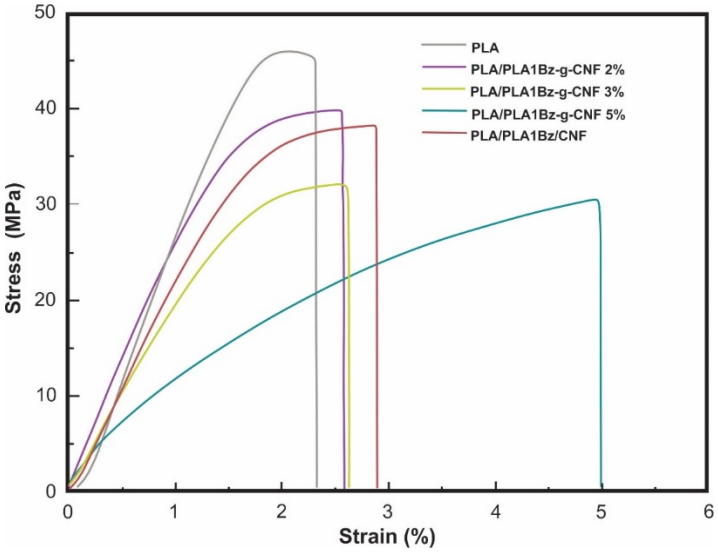

Fig. 8 Typical stress-strain curves for PLA and PLA nanocomposites.

Table 5. Mechanical properties for PLA and PLA nanocomposites

	Young's modulus (GPa)	**Tensile strength (MPa)**	**Elongation at break (%)**	**Work of fracture (MPa)**
Neat PLA	3.10±0.30	45.30±1.00	2.30±0.20	0.60±0.10
PLA/PLA1Bz-g-CNF 2%	2.80±0.20	39.59±0.50	2.59±0.20	0.64±0.10
PLA/PLA1Bz-g-CNF 3%	2.10±0.10	32.05±0.80	2.63±0.10	0.70±0.10
PLA/PLA1Bz-g-CNF 5%	1.50±0.10	30.28±0.80	5.00±0.30	0.98±0.20
PLA/PLA1Bz /CNF	2.40±0.30	38.31±3.10	2.90±0.20	0.75±0.10

The results showed that the addition of PLA1Bz-g-CNF changes the mechanical properties of the PLA film. As seen in **Table 5**, the elongation at break as well as the work of fracture increased progressively, while both the Young´s modulus and the tensile strength decreased. The addition of PLA1Bz-g-CNF 5% raised the elongation at break by

117% and the work of fracture by 63%, while in the blend the elongation at break increased by only 26%, which is still better than for PLA1Bz-g-CNF 2% (increase by 13%). The unexpected decrease in the stiffness observed when adding CNFs to the PLA matrix could be attributed to the decrease in the degree of crystallinity of the PLA matrix (**Table 4**). In addition, the grafting on CNFs or physical incorporation of low molecular weight PLA could act as a plasticizer for the PLA matrix.

3.3.4 Contact angle measurements

Table 6 shows the values of contact angle measured for water, diiodomethane and formamide deposited on PLA, PLA/PLA1Bz-g-CNF, and PLA/PLA1Bz/CNF films at longer times, i.e. when the equilibrium was reached.

Table 6. Contact angle values (°) of the tested liquids on PLA and PLA nanocomposites.

Sample	Water	Formamide	Diiodomethane
Neat PLA	76.6	54.5	45.9
PLA/PLA1Bz -g-CNF 2%	79.6	54.7	42.4
PLA/PLA1Bz -g-CNF 3%	80.7	57.1	40.7
PLA/PLA1Bz -g-CNF 5%	82.7	58.0	39.8
PLA/PLA1Bz /CNF	71.4	55.3	46.7

As seen in **Table 6**, a clear and progressive increase in the contact angle with water and formamide was observed when adding PLA1Bz-g-CNF in PLA. This result shows that the films become more hydrophobic after the addition of modified nanofibrils. The initial contact angle value for pure PLA was approximately 6° less than for the nanocomposite film reinforced with 5% PLA1Bz-g-CNF, while the mixture showed a contact angle of 71.9°, a value even lower than for neat PLA. This increase in hydrophobicity for the films loaded with PLA1Bz-g-CNF is attributed to the fact that the nanofibrils are covered almost entirely by small chains of PLA1 grafted onto their surface. Since all the nanofibrils are wrapped, their adhesion to the matrix should be improved, and it would produce a low exposure of available OH, generating a hydrophobic PLA surface. This would not happen

for the mixture, since the nanofibrils exhibit free OH available to interact with polar liquids (Bretas et al. 2015; Borkotoky et al. 2018).

For diiodomethane, an opposite behavior to that observed for the contact angle with water and formamide was reported for PLA/PLA1Bz-g-CNF, i.e. the contact angle progressively decreased when adding PLA1Bz-g-CNF. It confirms the effectiveness of the grafting method to decrease the hydrophilicity of the material compared to the physical blending (Labet et al. 2007; Habibi et al. 2008; Paquet et al. 2010).

3.3.5. Surface energy measurements

To further quantify the impact of the addition of nanofibrils to PLA, we determined the total surface energy (γ_S), together with the polar (γ_S^P) and dispersive (γ_S^D) components of the developed films (**Table 7**) using the constants of the solvents used as liquid probes (**Table 2**), according to the approach proposed by Owens and Wendt (Owens et al. 1969).

Table 7. Surface tension contributions for PLA and PLA nanocomposites.

Sample	γ_S^P (mN/m)	γ_S^D (mN/m)	γ_s (mN/m)
PLA	6.5	31.9	38.5
PLA/PLA1Bz-g-CNF 2%	4.6	34.7	39.3
PLA/PLA1Bz-g-CNF 3%	4.2	35.1	39.3
PLA/PLA1Bz -g-CNF 5%	3.1	36.1	39.3
PLA/PLA1Bz /CNF	9.7	29.3	38.9

When adding cellulose nanofibrils to the PLA matrix, the total surface energy did not change significantly. However, the addition of PLA1Bz-g-CNF progressively decreases the polar contribution γ_S^P to the surface energy. It is attributed to changes in the different intermolecular interaction like dipole-dipole, dipole-induced dipole and hydrogen bonding interactions indicating a decrease in wettability (Dhar et al. 2016). For PLA/PLA1Bz /CNF, an increase in the polar contribution to the surface energy is observed, which is an expected finding since the surface of CNFs contains OH-rich macromolecules, the most capable to establish hydrogen bonds. These results clearly show the difference in polarity between

PLA-grafted on CNFs and unmodified CNFs. It should directly affect the adhesion and dispersion of the filler in the PLA matrix, resulting in improvements in thermal and mechanical properties previously reported (Bendahou and Hajlane 2014).

3.3.6. Optical properties

The processing technology used in the present work allowed obtaining thin films prepared according to the formulations shown in **Table 1**, with thickness ranging between 26 and 27 μm.

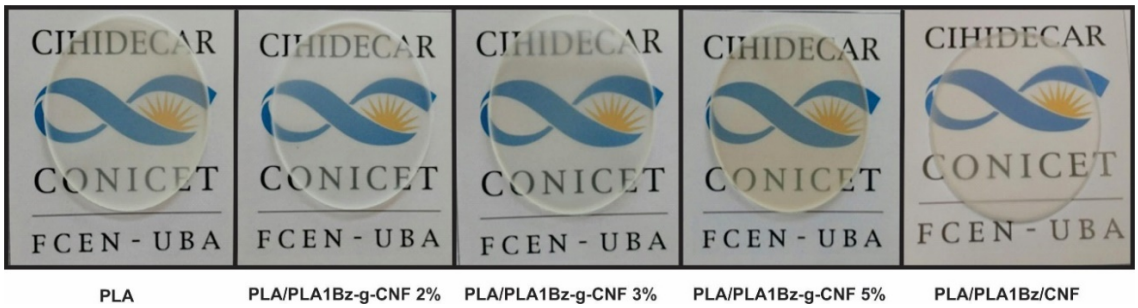

Fig. 9 Physical aspect of PLA, PLA/PLA1Bz -g-CNF and PLA/PLA1Bz /CNF films.

As the filler content in the material increased, the amber placement commonly found for PLA1Bz -g-CNF and PLA1Bz/CNF nanocomposites increased **(Figure 9**). On the other hand, this analysis does not allow observing significant differences between PLA1Bz -g-CNF and PLA1Bz /CNF nanocomposites.

Conclusions

Chemical grafting on CNFs with short PLA chains has been efficiently achieved and used in an attempt to obtain better compatibility by modifying the polar contribution to surface energy between the hydrophobic PLA matrix and the hydrophilic CNFs. The effect of the modified nanoparticles was tested by incorporating them into PLA matrix films. The results demonstrate the effect of modifying the CNFs by incorporating it into the PLA matrix, reducing the polar contributions of the nanofibrils in the films. As a result of this successful modification, an improvement was obtained in the thermal, mechanical and surface properties of the material. In particular, improvements in fracture work have been reported. This type of modification shows that it is possible, depending on the type of polymer grafted, to configure the properties of the films. The disposition of the OH

available in the nanofibrils can be adjusted according to the needs of the expected final properties. Finally, the physical-chemical, thermal, mechanical and surface properties evaluated in this study demonstrate the strong potential of biodegradable films as packaging materials in different industries, always taking into account the characteristics of the product to be packaged and the packaging requirements.

Acknowledgments

The authors acknowledge the financial support of UBACyT (No 20020130100021BA) and CONICET (PIP 112-2015-0100443CO). The authors thank Prof. Dr. Celina Bernal of the Faculty of Engineering, University of Buenos Aires for the use of the INSTRON 5982 dynamometer. LGP2 is part of the LabEx Tec 21 (Investissements d'Avenir - grant agreement n°ANR-11-LABX-0030) and of the PolyNat Carnot Institut (Investissements d'Avenir - grant agreement n°ANR-11-CARN-030-01).

References

Adamson AW, Gast AP (1990) Physical Chemistry of Surfaces Sixth Edition, Sixth Edit. New York

Aitomäki Y, Mathew AP, Siqueira G, et al (2016) Review of the recent developments in cellulose nanocomposite processing. Compos Part A Appl Sci Manuf 83:2–18. https://doi.org/10.1016/j.compositesa.2015.10.041

Aouat T, Kaci M, Devaux E, et al (2018) Morphological, Mechanical, and Thermal Characterization of Poly(Lactic Acid)/Cellulose Multifilament Fibers Prepared by Melt Spinning. Adv Polym Technol 37:1193–1205. https://doi.org/10.1002/adv.21779

Bendahou A, Hajlane A (2014) Esterification and amidation for grafting long aliphatic chains on to cellulose nanocrystals : a comparative study. Res Chem Intermed 41:4293–4310. https://doi.org/10.1007/s11164-014-1530-z

Bondeson D, Oksman K (2007) Dispersion and characteristics of surfactant modified cellulose whiskers nanocomposites. Compos Interfaces 14:617–630. https://doi.org/10.1163/156855407782106519

Borkotoky SS, Chakraborty G, Katiyar V (2018) Thermal degradation behaviour and crystallization kinetics of poly (lactic acid) and cellulose nanocrystals (based microcellular composite foams. Int J Biol Macromol 118:1518–1531. https://doi.org/10.1016/j.ijbiomac.2018.06.202

Bretas ES, Crisci A, Bras J (2015) Supramolecular aromatic interactions to enhance biodegradable film properties through incorporation of functionalized cellulose nanocrystals. Compos Part A Appl Sci Manuf 83:80–88. https://doi.org/https://doi.org/10.1016/j.compositesa.2015.10.038

C. A. Rodríguez Ramírez, Rol F, Bras J, et al (2019) Isolation and Characterization of Cellulose Nanofibers from Argentine Tacuara Cane (Guadua Angustifolia Kunth). J Renew Mater 7:373–381. https://doi.org/10.32604/jrm.2019.04236

Carlmark A, Larsson E, Malmström E (2012) Grafting of cellulose by ring-opening polymerisation – A review. Eur Polym J 48:1646–1659. https://doi.org/10.1016/j.eurpolymj.2012.06.013

Corrêa AC, de Teixeira EM, Pessan LA, Mattoso LHC (2010) Cellulose nanofibers from curaua fibers. Cellulose 17:1183–1192. https://doi.org/10.1007/s10570-010-9453-3

Dhar P, Bhasney SM, Kumar A, Katiyar V (2016) Acid functionalized cellulose nanocrystals and its effect on mechanical , thermal , crystallization and surfaces properties of poly (lactic acid) bionanocomposites fi lms : A comprehensive study. Polymer (Guildf) 101:75–92. https://doi.org/10.1016/j.polymer.2016.08.028

Fukushima K, Furuhashi Y, Sogo K, et al (2005) Stereoblock Poly (lactic acid): Synthesis via Solid-State Polycondensation of a Stereocomplexed Mixture of Poly (L -lactic acid) and Poly (D -lactic acid). Macromol Biosci 5:21–29. https://doi.org/10.1002/mabi.200400121

García NL, Lamanna M, D'Accorso N, et al (2012) Biodegradable materials from grafting of modified PLA onto starch nanocrystals. Polym Degrad Stab 97:2021–2026. https://doi.org/10.1016/j.polymdegradstab.2012.03.032

Georgopoulos ST, Tarantili PA, Avgerinos E, et al (2005) Thermoplastic polymers reinforced with fibrous agricultural residues. Polym Degrad Stab 90:303–312. https://doi.org/10.1016/j.polymdegradstab.2005.02.020

Gorade VG, Kotwal A, Chaudhary BU, Kale RD (2019) Surface modification of microcrystalline cellulose using rice bran oil: a bio-based approach to achieve water repellency. J Polym Res 26:. https://doi.org/10.1007/s10965-019-1889-z

Habibi Y, Goffin A, Schiltz N, et al (2008) Bionanocomposites based on poly (3 - caprolactone) -grafted cellulose nanocrystals by ring-opening polymerization. J Mater Chem 18:5002–5010. https://doi.org/10.1039/b809212e

Inácio EM, Souza DHS, Dias ML (2020) Thermal and Crystallization Behavior of PLA / PLLA-Grafting Cellulose Nanocrystal. Mater Sci Appl 11:44–57. https://doi.org/10.4236/msa.2020.111004

Jamshidian M, Tehrany EA, Imran M, et al (2010) Poly-Lactic Acid: Production, applications, nanocomposites, and release studies. Compr Rev Food Sci Food Saf 9:552–571. https://doi.org/10.1111/j.1541-4337.2010.00126.x

Kopinke FD, Remmler M, Mackenzie K, et al (1996) Thermal decomposition of biodegradable polyesters - II. Poly(lactic acid). Polym Degrad Stab 53:329–342. https://doi.org/10.1016/0141-3910(96)00102-4

Kunaver M, Anžlovar A, Žagar E (2016) The fast and effective isolation of nanocellulose from selected cellulosic feedstocks. Carbohydr Polym 148:251–258. https://doi.org/10.1016/j.carbpol.2016.04.076

Kwak HW, Lee H, Lee ME, Jin HJ (2018) Facile and green fabrication of silk sericin films reinforced with bamboo-derived cellulose nanofibrils. J Clean Prod 200:1034–1042. https://doi.org/10.1016/j.jclepro.2018.07.289

La Mantia FP, Morreale M (2011) Green composites: A brief review. Compos Part A Appl Sci Manuf 42:579–588. https://doi.org/10.1016/j.compositesa.2011.01.017

Labet M, Thielemans W, Dufresne A (2007) Polymer grafting onto starch nanocrystals.

Biomacromolecules 8:2916–2927. https://doi.org/10.1021/bm700468f

Lv Q, Xu C, Wu D, et al (2017) Composites : Part A The role of nanocrystalline cellulose during crystallization of poly (e -caprolactone) composites : Nucleation agent or not ? Compos Part A 92:17–26. https://doi.org/10.1016/j.compositesa.2016.10.035

Ly B, Thielemans W, Dufresne A, et al (2008) Surface functionalization of cellulose fibres and their incorporation in renewable polymeric matrices. Compos Sci Technol 68:3193–3201. https://doi.org/10.1016/j.compscitech.2008.07.018

Maisa Milanez Ávila Dias Maciel, Kelly Cristina Coelho de Carvalho Benini, Herman Jacobus Cornelis Voorwald MOHC (2019) Obtainment and characterization of nanocellulose from an unwoven industrial textile cotton waste: Effect of acid hydrolysis conditions. Int J Biol Macromol 126:496–506. https://doi.org/10.1016/j.ijbiomac.2018.12.202

Mao J, Tang Y, Zhao R, et al (2019) Preparation of nanofibrillated cellulose and application in reinforced PLA/starch nanocomposite film. J Polym Environ 27:728–738. https://doi.org/10.1007/s10924-019-01382-6

Minh T, Hoa H, Ngoc P (2013) Stereocomplexation of low molecular weight poly (L-lactic acid) and high molecular weight poly (D-lactic acid), radiation crosslinking PLLA / PDLA stereocomplexes and their characterization. Radiat Phys Chem 83:105–110. https://doi.org/10.1016/j.radphyschem.2012.10.002

Missoum K, Bras J, Belgacem MN (2012) Organization of aliphatic chains grafted on nanofibrillated cellulose and influence on final properties. Cellulose 19:1957–1973. https://doi.org/10.1007/s10570-012-9780-7

Oun AA, Rhim JW (2016) Characterization of nanocelluloses isolated from Ushar (Calotropis procera) seed fiber: Effect of isolation method. Mater Lett 168:146–150. https://doi.org/10.1016/j.matlet.2016.01.052

Owens DK, Nemours EIP De, Film S (1969) Estimation of the Surface Free Energy of Polymers. J Appl Polym Sci 13:1741–1747.

https://doi.org/https://doi.org/10.1002/app.1969.070130815

Paquet O, Krouit M, Bras J, et al (2010) Surface modification of cellulose by PCL grafts. Acta Mater 58:792–801. https://doi.org/10.1016/j.actamat.2009.09.057

Piemonte V, Gironi F (2013) Kinetics of Hydrolytic Degradation of PLA. J Polym Environ 21:313–318. https://doi.org/10.1007/s10924-012-0547-x

Quero E, Müller AJ, Signori F, et al (2012) Isothermal cold-crystallization of PLA/PBAT blends with and without the addition of acetyl tributyl citrate. Macromol Chem Phys 213:36–48. https://doi.org/10.1002/macp.201100437

Ray D, Sain S (2016) In situ processing of cellulose nanocomposites. Compos Part A Appl Sci Manuf 83:19–37. https://doi.org/10.1016/j.compositesa.2015.09.007

Rol F, Banvillet G, Meyer V, et al (2018) Combination of twin-screw extruder and homogenizer to produce high-quality nanofibrillated cellulose with low energy consumption. J Mater Sci 53:12604–12615. https://doi.org/10.1007/s10853-018-2414-1

Sajan D, Hubert Joe I, Jayakumar VS (2006) NIR-FT Raman, FT-IR and surface-enhanced Raman scattering spectra of organic nonlinear optic material: p-hydroxy acetophenone. J Raman Spectrosc 37:508–519. https://doi.org/10.1002/jrs.1424

Scaffaro R, Botta L, Lopresti F, et al (2017) Polysaccharide nanocrystals as fillers for PLA based nanocomposites. Cellulose 24:447–478. https://doi.org/10.1007/s10570-016-1143-3

Shojaeiarani J, Bajwa DS, Hartman K (2019) Esterified cellulose nanocrystals as reinforcement in poly(lactic acid) nanocomposites. Cellulose 4:. https://doi.org/10.1007/s10570-018-02237-4

Souza AG de, Rocha DB, Kano FS, Rosa D dos S (2019) Valorization of industrial paper waste by isolating cellulose nanostructures with different pretreatment methods. Resour Conserv Recycl 143:133–142. https://doi.org/10.1016/j.resconrec.2018.12.031

Suryanegara L, Nakagaito AN, Yano H (2009) The effect of crystallization of PLA on the thermal and mechanical properties of microfibrillated cellulose-reinforced PLA composites. Compos Sci Technol 69:1187–1192. https://doi.org/10.1016/j.compscitech.2009.02.022

Tingaut P, Zimmermann T, Lopez-Suevos F (2010) Synthesis and characterization of bionanocomposites with tunable properties from poly(lactic acid) and acetylated microfibrillated cellulose. Biomacromolecules 11:454–464. https://doi.org/10.1021/bm901186u

Trinh BM, Mekonnen T (2018) Hydrophobic Esterification of Cellulose Nanocrystals for Epoxy Reinforcement. Polymer (Guildf). https://doi.org/10.1016/j.polymer.2018.08.076

Wang S, Dai G, Yang H, Luo Z (2017) Lignocellulosic biomass pyrolysis mechanism: A state-of-the-art review. Prog Energy Combust Sci 62:33–86. https://doi.org/10.1016/j.pecs.2017.05.004

Wu H, Nagarajan S, Zhou L, et al (2016) Synthesis and characterization of cellulose nanocrystal-graft-poly(D-lactide) and its nanocomposite with poly(L-lactide). Polymer (Guildf) 103:365–375. https://doi.org/10.1016/j.polymer.2016.09.070

Yu J, Ai F, Dufresne A, et al (2008) Structure and Mechanical Properties of Poly (lactic acid) Filled with (Starch nanocrystal) -graft- poly (e -caprolactone). Macromol Mater Eng 293:763–770. https://doi.org/10.1002/mame.200800134

Zamir SS, Frouzanmehr MR, Nagalakshmaiah M, et al (2018) Chemical compatibility of lactic acid-grafted starch nanocrystals (SNCs) with polylactic acid (PLA). Polym Bull. https://doi.org/10.1007/s00289-018-2548-y

Funding

The financial support of UBACyT (No 20020130100021BA) and CONICET (PIP 112-2015-0100443CO). LGP2 is part of the LabEx Tec 21 (Investissements d'Avenir -

grant agreement n°ANR-11-LABX-0030) and of the PolyNat Carnot Institut (Investissements d'Avenir - grant agreement n°ANR-11-CARN-030-01).

Declaration of interests

The authors declare that they have no known competing financial interests or personal relationships that could have appeared to influence the work reported in this paper.

Availability of data and material

Available on demand to author

Code availability

No Applicable.

Authors' contributions

Nancy Lis Garcia: Conceptualization, Methodology, Resources, Investigation, Validation, Writing - Review & Editing

Norma D'Accorso: Conceptualization, Supervision, Project administration, Funding acquisition, Resources

Alain Dufresne: Supervision, Writing - Review & Editing

Carlos A. Rodriguez: Investigation, Writing - Original Draft, Data Curation.

Figures

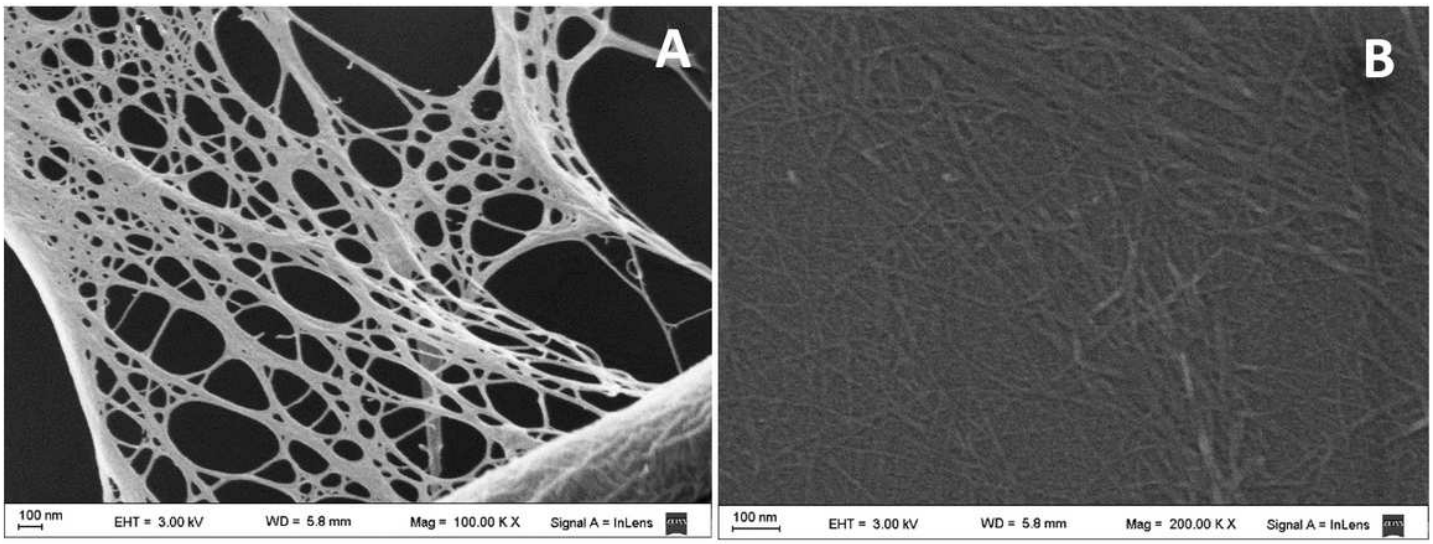

Figure 1

FESEM of A, B. CNFs Tacuara Cane, with different magnifications, A: 100.00 KX and B: 200 KX

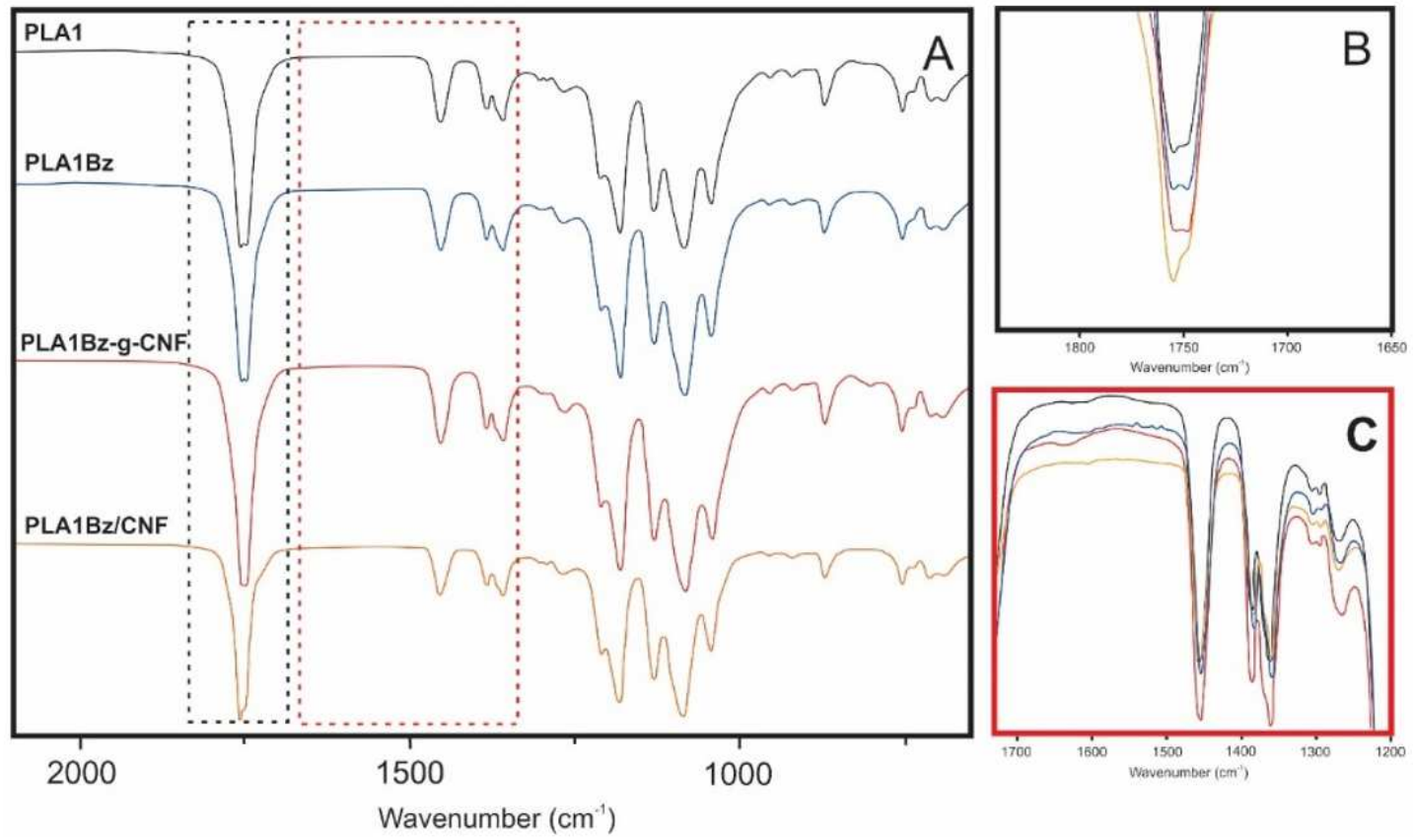

Figure 2

(A) ATR-FTIR for PLA1, PLA1Bz, PLA1Bz-g-CNF and PLA1Bz/CNF; (B) expanded view of the band near 1750 cm-1; (C) expanded view of the spectra in the 1700-1200 cm-1 wavenumber range.

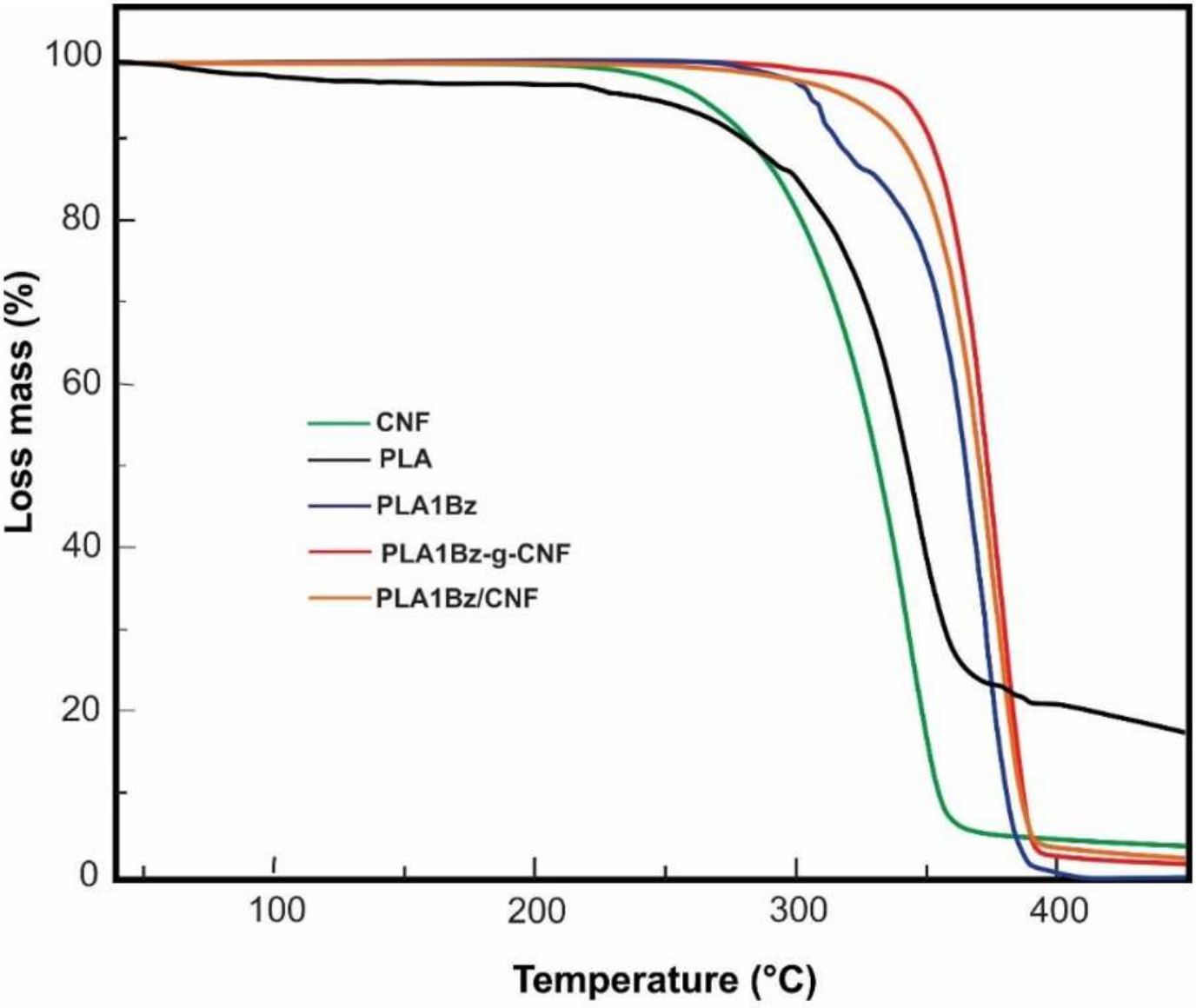

Figure 3

Thermogravimetric analysis for PLA1, CNF, PLA1Bz, PLA1Bz-g-CNF, and PLA1Bz/CNF

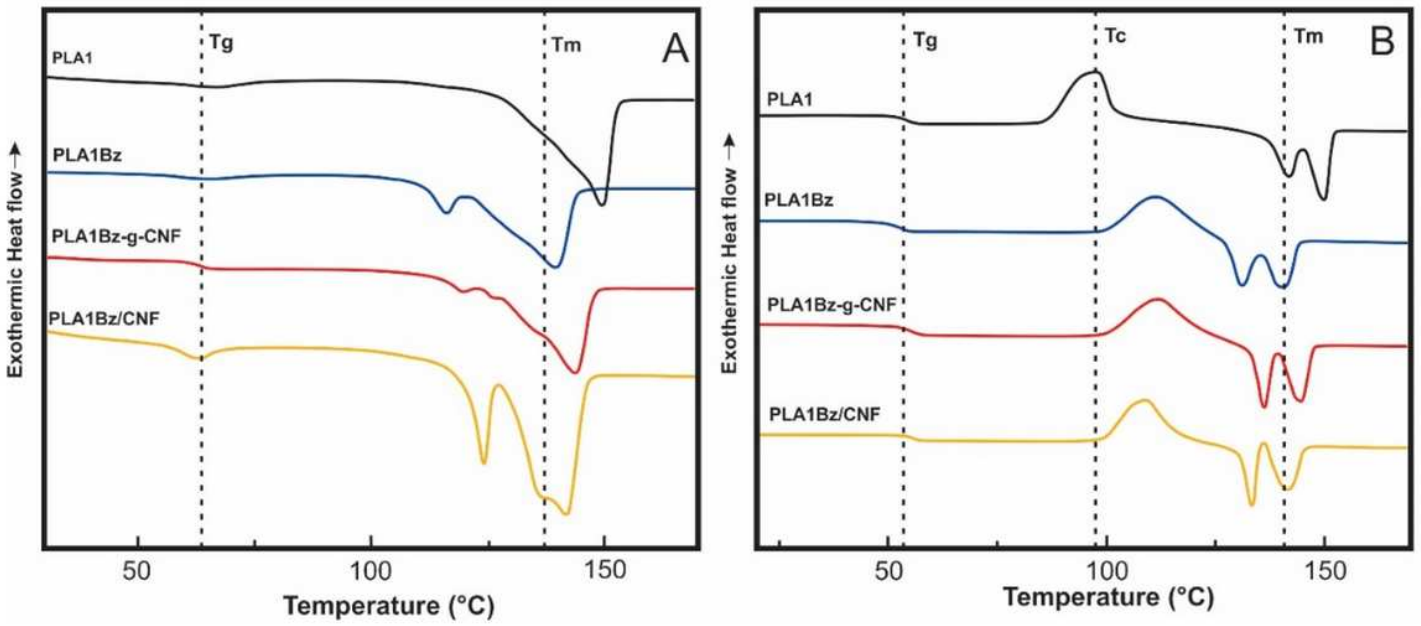

Figure 4

DSC analysis for PLA1, CNF, PLA1Bz, PLA1Bz-g-CNF, and PLA1Bz/CNF: (A) first heating scan, and (B) second heating scan.

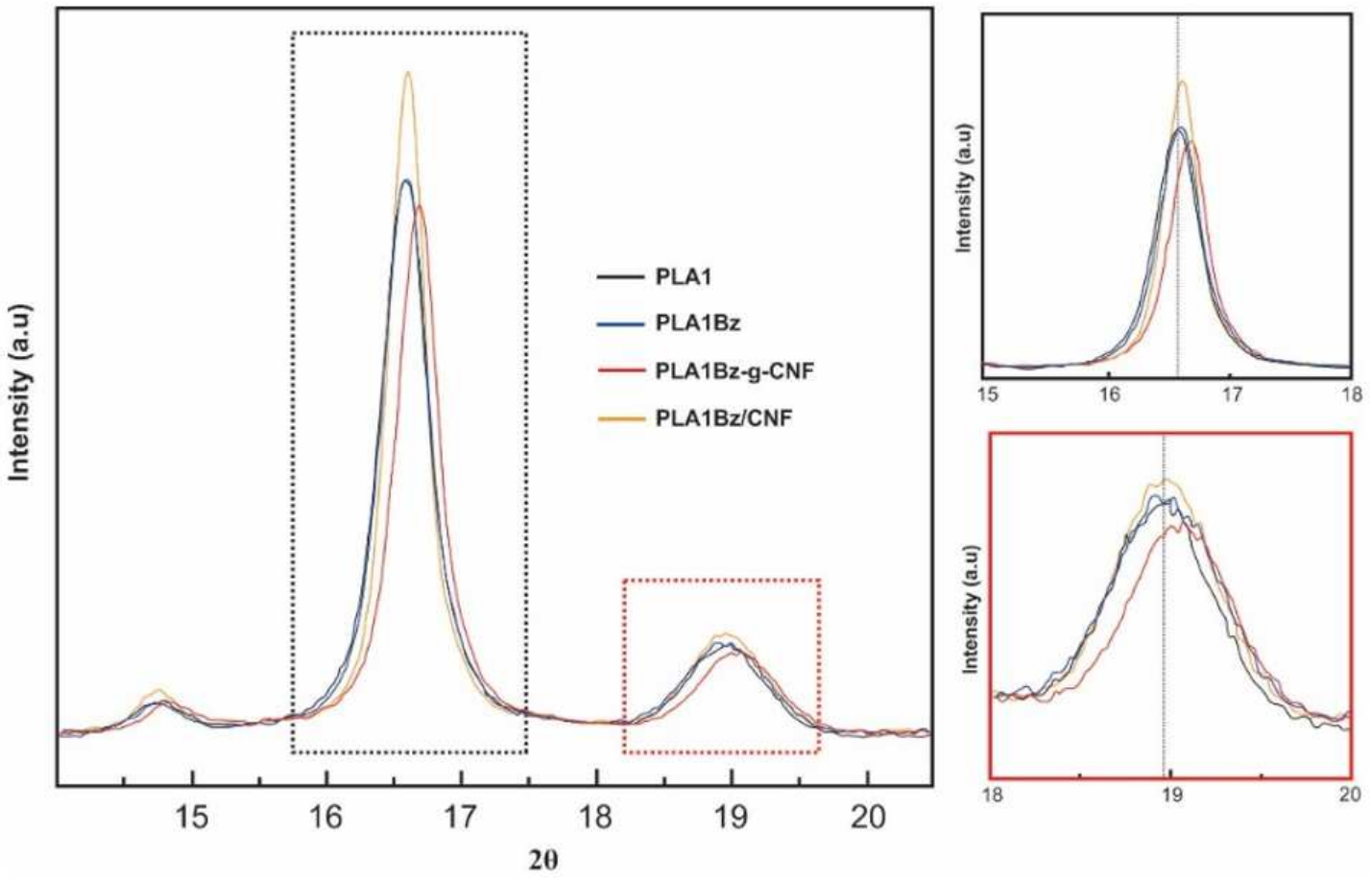

Figure 5

XRD patterns for PLA1, PLA1Bz, PLA1Bz-g-CNF and PLA1Bz/CNF.

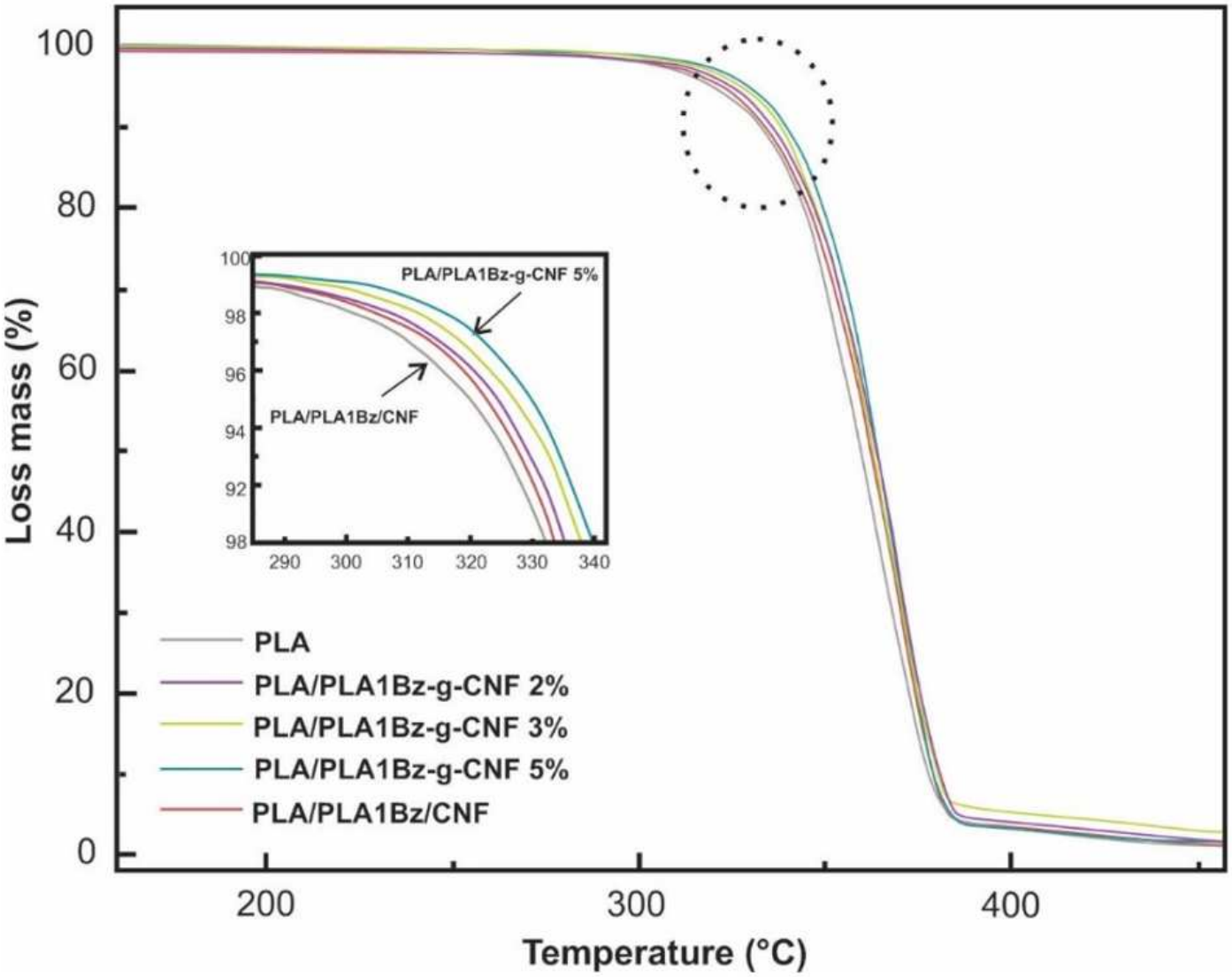

Figure 6

TGA curves for neat PLA, PLA/PLA1Bz-g-CNF and PLA/PLA1Bz/CNF films.

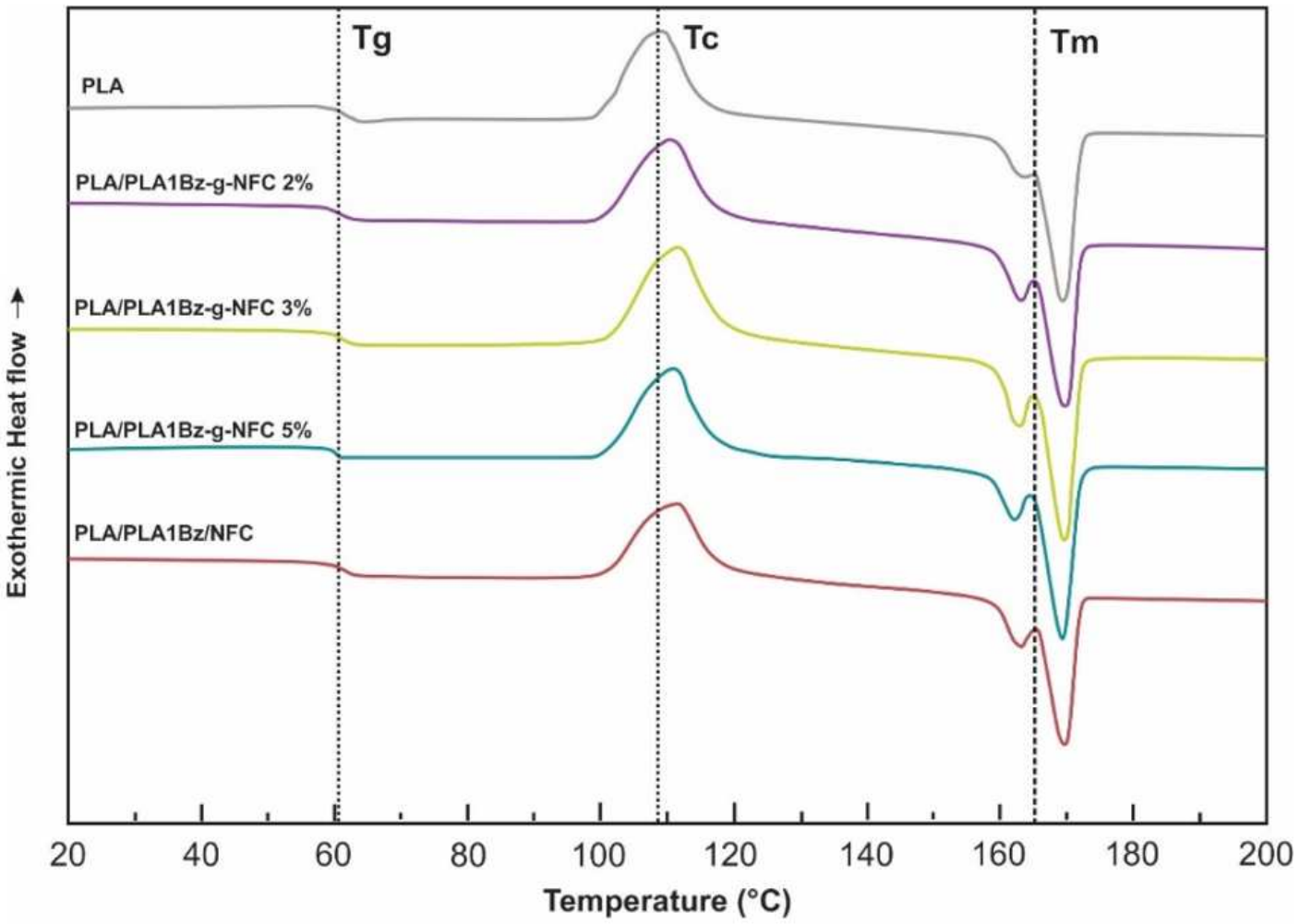

Figure 7

DSC thermograms for neat PLA and PLA nanocomposites.

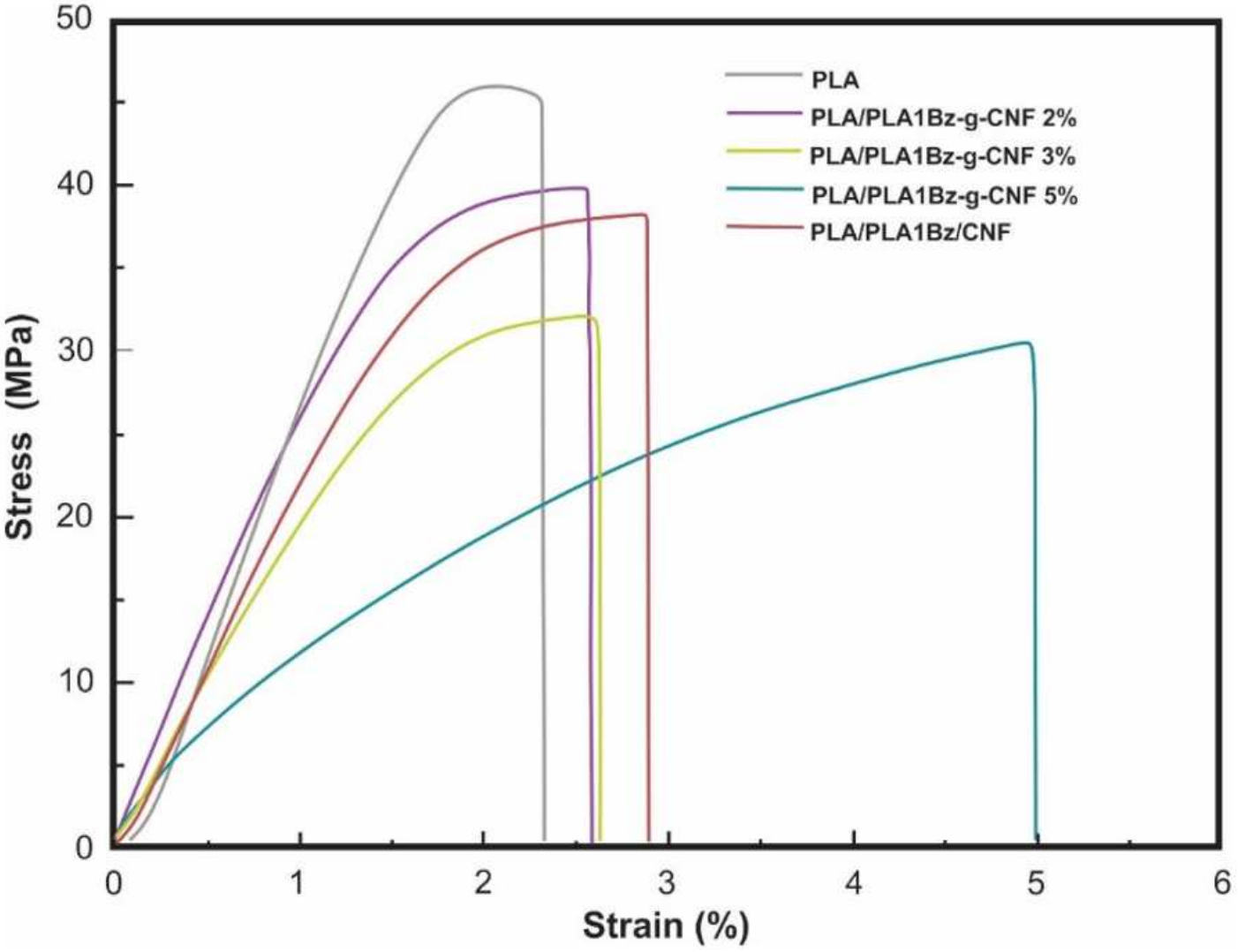

Figure 8

Typical stress-strain curves for PLA and PLA nanocomposites.

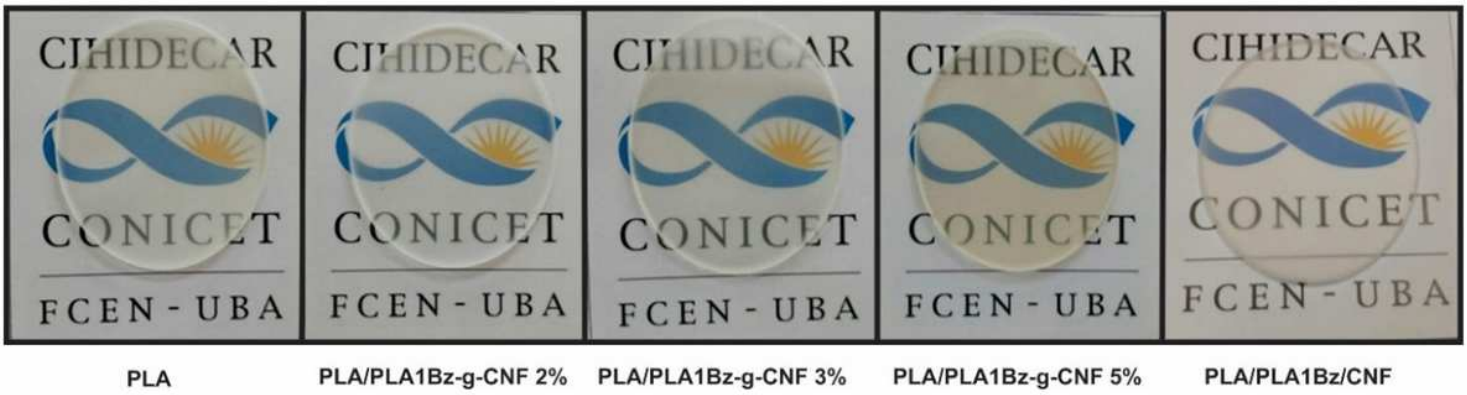

Figure 9

Physical aspect of PLA, PLA/PLA1Bz -g-CNF and PLA/PLA1Bz /CNF films.